Check for updates

View Article Online
View Journal

NJC

Accepted Manuscript

This article can be cited before page numbers have been issued, to do this please use: J. Xu, Y. Wang, Y. Cao, Z. He, L. Zhao, U. J. ETIM, P. Bai, Z. Yan and P. Wu, *New J. Chem.*, 2019, DOI: 10.1039/C8NJ05642K.

Volume 40 | Number 1 | January 2016 | Pages 1–846

NJC

New Journal of Chemistry
www.rsc.org/njc

A journal for new directions in chemistry

ISSN 1144-0546

ROYAL SOCIETY OF CHEMISTRY

PAPER
Jason B. Benedict *et al.*
The role of atropisomers on the photo-reactivity and fatigue of diarylethene-based metal–organic frameworks

This is an Accepted Manuscript, which has been through the Royal Society of Chemistry peer review process and has been accepted for publication.

Accepted Manuscripts are published online shortly after acceptance, before technical editing, formatting and proof reading. Using this free service, authors can make their results available to the community, in citable form, before we publish the edited article. We will replace this Accepted Manuscript with the edited and formatted Advance Article as soon as it is available.

You can find more information about Accepted Manuscripts in the author guidelines.

Please note that technical editing may introduce minor changes to the text and/or graphics, which may alter content. The journal's standard Terms & Conditions and the ethical guidelines, outlined in our author and reviewer resource centre, still apply. In no event shall the Royal Society of Chemistry be held responsible for any errors or omissions in this Accepted Manuscript or any consequences arising from the use of any information it contains.

ROYAL SOCIETY OF CHEMISTRY

rsc.li/njc

NJC

View Article Online
DOI: 10.1039/C8NJ05642K

PAPER

What is the Effect of Sn and Mo oxides on Gold Catalyst for Selective Oxidation of Benzyl Alcohol?

Received 00th January 20xx,
Accepted 00th January 20xx

DOI: 10.1039/x0xx00000x

www.rsc.org/

Jing Xu,[a] Yue Wang, [b] Yunxiang Cao, [b] Zhengke He, [b] Lianming Zhao, [a] Ubong Jerome Etim, [b] Peng Bai,[b] Zifeng Yan, [b] Pingping Wu [b] *

A foam-liked mesoporous silica (MCF) supported gold (Au) nanoparticle (NP) catalyst was prepared by a facile one-pot synthesis strategy. SnO_x and MoO_x were introduced as promoters by wet impregnation method to synthesize promoted catalysts Au-SnO_x/MCF and Au-MoO_x/MCF, respectively. The evaluation of prepared catalysts in benzyl alcohol oxidation shows that introduction of a low amount of SnO_x (0.2 wt.%) lead to a higher catalytic activity, while a relatively high amount of SnO_x (1.0 wt%) has lower catalytic activity than the unpromoted Au NP catalyst. Both characterization results and density functional theory (DFT) calculation suggest that the most important effect of SnO_x species on gold catalyst is the strong interaction between them which leads to the electrons transfer and lattice distortion of Au NPs, providing more low-coordinated Au active sites. This structural modification enhanced the chemisorption of reactants and lowers the energy barrier for the dissociation of O_2 molecules on the surface of gold catalyst, improving the catalytic performance for benzyl alcohol oxidation. However, a weaker interaction was detected between MoO_x and Au NPs on catalyst Au-MoO_x/MCF and no lattice modification was observed, thus no improvement of catalytic activity for benzene alcohol oxidation occurred on catalyst Au-MoO_x/MCF.

Introduction

The selective catalytic oxidation of benzyl alcohols is of paramount interest in industry, due to the huge demand for benzaldehydes and benzoic acids as important intermediates in pharmaceuticals, fragrances, and flavoring additives.[1-5] Homogeneous acid catalysts (such as heteropoly tungstates and heteropoly molybdate) are generally used to synthesize benzaldehydes and benzoic acids in industry,[6, 7] which is not convenient for large-scale production and usually causes serious pollution. So it is urgent to find an economical and environmentally friendly heterogeneous catalyst to replace homogeneous ones.

Heterogeneous catalysis is promising in industrial processes due to its simple operation flow and easy separation of products from catalysts.[8] In 1987, Haruta et al. found that the supported gold catalyst showed high catalytic activity for CO oxidation at -70 °C and was stable in a moistened gas atmosphere. [9] Subsequent studies further confirm that gold catalysts have excellent catalytic activity in partial oxidation of organic compounds.[10-16] Yoskamtorn reported that the supported Au_{25} clusters prepared by the sol-gel method were effective catalysts for the aerobic oxidation of benzyl alcohol. [17]

Furthermore, bimetallic gold (Au) and palladium (Pd) catalysts have been widely used in alcohol oxidation and the combination of Au and Pd as alloy NPs show enhanced catalytic activity for the oxidation of benzyl alcohol.[18-23] However, the selectivity of the catalyst to benzaldehyde is low, with a significant amount of by-product toluene. In order to improve the selectivity of benzaldehyde on gold catalyst, transition metal oxides are used as supports or auxiliary components. On the other hand, the introduction of transition metals or their oxides into gold NP catalysts can change the surface electronic properties of gold catalysts and effectively improve the stability and activity of gold NP catalysts.[24-26] Della et al. [27] reported that the introduction of Cu effectively dispersed Au NPs and improved the stability of the NP catalyst. Silica-supported Au-Cu alloy catalyst exhibited good activity for oxidation of benzyl alcohol in air, affording benzaldehyde with high selectivity and high yield. [27, 28] Yi et al. [29] synthesized an Au-Ni bimetallic catalyst with excellent catalytic activity for the oxidation of benzyl alcohol in gas phase, and the improved selectivity to benzaldehyde (over 99%). The superior activities of these Au-Cu and Au-Ni catalysts were attributed to the presence of transition metal oxides (CuO_x and NiO_x) on the transition metal oxides-Au interfaces.[25, 29] Therefore, transition metals or their oxides are a good choice to promote gold catalysts for selective benzyl alcohol oxidation, however, the mechanistic effect of these transition metal oxides on Au NP catalyst was seldom studied.

In this work, a foam-liked mesoporous silica (MCF) supported Au NP catalyst was prepared by a one-pot synthesis strategy. And subsequently, transition metal oxides, tin oxide (SnO_x) and molybdenum oxide (MoO_x) were introduced as an auxiliary

---

[a] *State Key Laboratory of Heavy Oil Processing, School of Materials Science and Engineering, Institute of Advanced Materials, China University of Petroleum (East China), Qingdao, Shandong 266580, China.*
[b] *State Key Laboratory of Heavy Oil Processing, Key Laboratory of Catalysis, College of Chemical Engineering, China University of Petroleum (East China), Qingdao 266580, China*
Tel: 86-532-86984615. E-mail: wupp@upc.edu.cn (Wu P).

View Article Online
DOI: 10.1039/C8NJ05642K

components by wet impregnation method to synthesize catalysts Au-SnO_x/MCF and Au-MoO_x/MCF, respectively. The effects of transition metal oxides on the structure and catalytic performance of Au NPs have been systematically explored and theoretically validated. This study suggests a theoretical basis for the preparation of highly efficient transition metal oxide promoted Au NP catalyst.

Results and Discussion

Physicochemical properties

The N_2 absorption-desorption isotherms and pore size distribution curves of catalysts Au-SnO_x/MCF and Au-MoO_x/MCF are shown in Fig. 1 and the results are summarized in Table 1. Both Au-SnO_x/MCF and Au-MoO_x/MCF samples have a typical type IV isotherm with a H-2 hysteresis loop, indicating a typical ink-bottle mesoporous structure for all catalysts, similar to pristine MCF.[30] As shown in Fig. 1, all samples have similar pore size distribution in the range of 3.4~4.8 nm. The introduction of transition oxides has no significant effect on the mesoporous structure of the catalysts, mirrored by the N_2 absorption/desorption isotherms and the pore size distribution curves. After loading transition metal oxides, the specific surface areas of the catalyst are slightly lower than those of pure Au/MCF catalyst, but still as large as 726.7~793.6 m^2g^{-1} and 596.1~659.1 m^2g^{-1} for Au-SnO_x/MCF and Au-MoO_x/MCF catalysts, respectively. In addition, compared to Sn, the Mo component with higher oxidation state occupies larger volume of catalyst pores, resulting in a lower specific surface areas of Au-MoO_x/MCF.

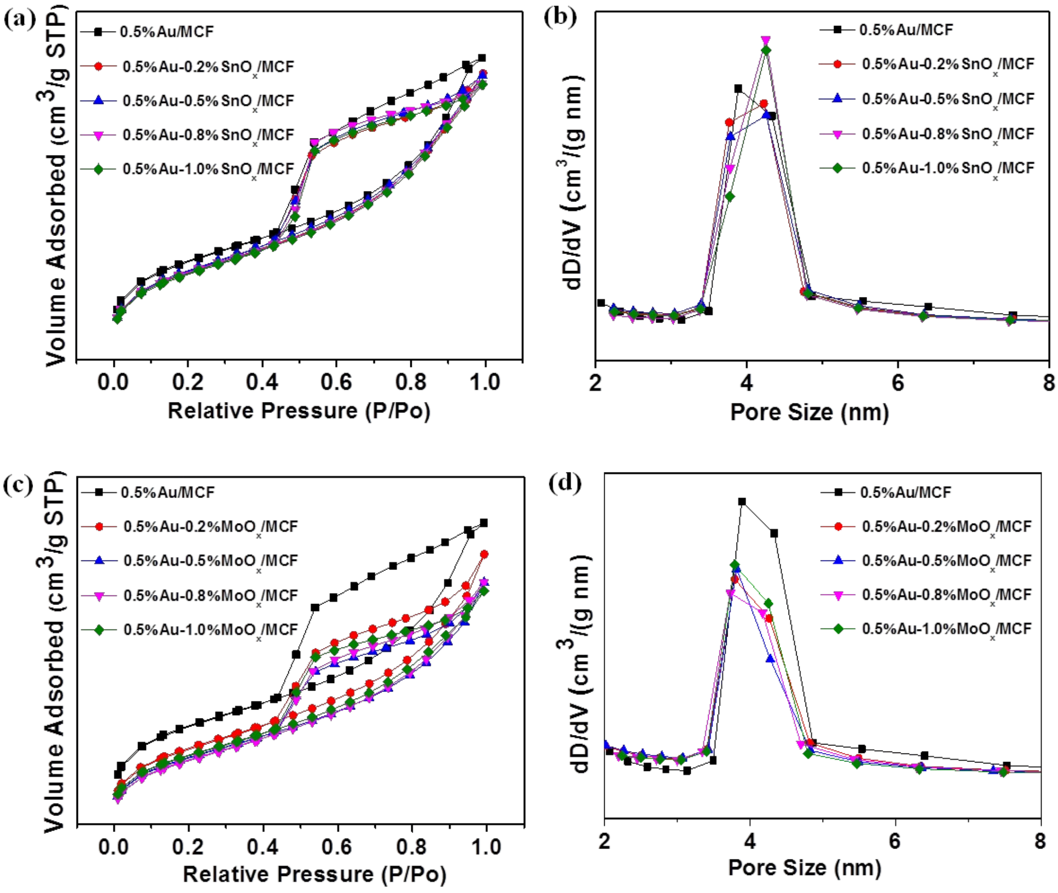

Fig. 1 N_2 adsorption-desorption isotherms (left) and pore size distribution curves (right) of (a) and (b) Au-SnO_x/MCF and (c) and (d) Au-MoO_x/MCF.

The morphologies of the prepared catalysts were characterized by TEM (see Fig. 2). As shown in Fig.2, the catalyst support shows a distinct foamed silica structure for all prepared samples, indicating that the introduction of metal ions in the preparation process does not have a significant effect on the morphology of the catalyst support. It is also seen that the metal NPs uniformly distributed on the surface and in the pores of the support. For 0.5%Au/MCF, the average particle diameter is 1.9±0.45 nm with a narrow particle size distribution of 1-4 nm. After loading transition metal oxides, the dispersion of the NPs is lowered, and the particle size increased to 6.6±0.45 and 5.1±0.45 nm for 0.5%Au-0.2%SnO_x/MCF and 0.5%Au-0.2%MoO_x/MCF, respectively, indicating that the introduction of transition metal oxide results in the agglomeration of Au NPs to some extent. The bulk and surface Sn(Mo)/Au content was characterized by inductively coupled plasma optical emission spectroscopy (ICP-OES) and X-ray photoelectron spectroscopy (XPS), respectively, as shown in Table 1. The surface Sn/Au ratio was always higher than that in bulk because the transition metal was introduced by impregnation method to one-pot synthesized 0.5%Au /MCF. On catalysts 0.5%Au-0.2%SnO_x/MCF, the difference of surface and bulk Sn/Au ratio was

View Article Online
DOI: 10.1039/C8NJ05642K

small, however, this difference is growing up with the increase of transition metal loading, indicating that the surface Au atoms were covered by transition metal oxide.

Table 1 Textural properties of catalysts.

Catalysts	BET surface area (m^2 g^{-1})	Pore volume (cm^3g^{-1})	Mean pore size (nm)	Au $d_{(111)}$ (nm)	Atomic ratio	
					ICP Sn(Mo)/Au	XPS Sn(Mo)/Au
0.5%Au/SiO_2	793.2	0.95	5.5	0.2351	--	--
0.5%Au-0.2%SnO_x/SiO_2	726.7	0.90	4.9	0.2359	0.69	0.89
0.5%Au-0.5%SnO_x/SiO_2	737.3	0.90	4.8	0.2360	1.72	4.32
0.5%Au-0.8%SnO_x/SiO_2	729.6	0.87	4.8	0.2359	2.77	10.25
0.5%Au-1.0%SnO_x/SiO_2	723.6	0.87	4.8	0.2358	3.44	21.10
0.5%Au-0.2%MoO_x/SiO_2	659.1	0.86	5.1	--	0.86	--
0.5%Au-0.5%MoO_x/SiO_2	601.6	0.78	5.1	0.2351	2.14	--
0.5%Au-0.8%MoO_x/SiO_2	596.1	0.78	5.2	0.2350	3.42	--
0.5%Au-1.0%MoO_x/SiO_2	621.8	0.75	4.8	0.2351	4.28	--

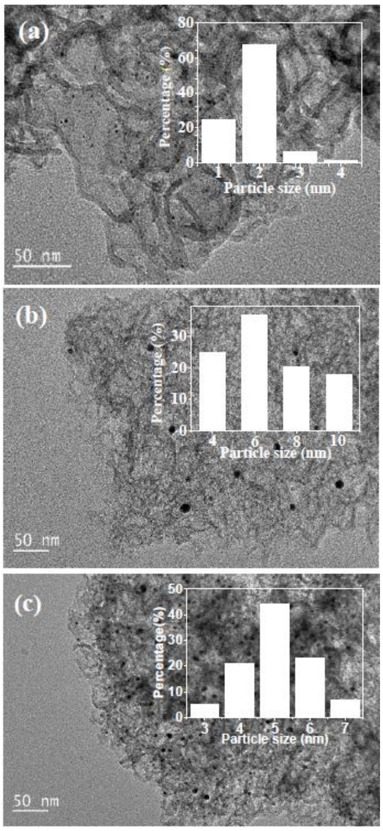

Fig. 2 TEM images and particles size distribution histograms of (a) 0.5%Au /MCF, (b) 0.5%Au-0.2%SnO_x/MCF, and (c) 0.5%Au-0.2%MoO_x/MCF.

Wide-angle XRD patterns of Au/MCF, Au-SnO_x/MCF, and Au-MoO_x/MCF catalysts shown in Fig. 3 confirmed the TEM results.

Sample 0.5%Au/MCF shows no obvious diffraction peaks at 2θ = 38.25°, 44.46°, 64.69°, and 77.72°, which corresponds to the diffractions of the (111), (200), (220), (311) planes of cubic Au (PDF#65-8601), respectively. This indicates that the gold NPs are evenly distributed on the MCF surface. After introducing SnO_x to Au/MCF, four diffraction peaks were observed on catalysts Au-SnO_x/MCF, but the diffraction peak positions of Au-SnO_x/MCF is slightly shifted toward low angles, compared to the 0.5%Au/MCF catalyst. Therefore, according to the Bragg equation, the crystal inter-planar spacing of the cubic Au(111) is increased in Au-SnO_x/MCF, due to the interaction between SnO_x and Au NPs. The lattice spacing of the (111) plane is calculated to be 0.2351, 0.2359, 0.2360, 0.2359, and 0.2358 nm for 0.5%Au/MCF, 0.5%Au-0.2%SnO_x/MCF, 0.5%Au-0.5%SnO_x/MCF, 0.5%Au-0.8%SnO_x/MCF, and 0.5%Au-1.0%SnO_x/MCF, respectively, indicating a distortion of the lattice spacing with the SnO_x introduced (as shown in Table 1). In addition, all the calculated lattice spacing of Au-SnO_x/MCF are larger than that of Au/MCF, further confirming that the addition of SnO_x caused an increase in the inter-planar spacing of gold. Compared to 0.5%Au/MCF, the intensity of the diffraction peaks for Au-SnO_x/MCF is increased, indicating that the introduction of tin oxide increases the size of the gold NPs. This is well consistent with the TEM results (Fig. 2). After introducing molybdenum oxide to Au/MCF, the intensity of the four diffraction peaks for cubic gold phase slightly enhanced on catalyst Au-MoO_x/MCF but not as high as those on catalysts Au-SnO_x/MCF. Moreover, compared to 0.5%Au/MCF, no obvious change in XRD spectra of Au-MoO_x/MCF was observed, suggesting that the introduction of molybdenum oxide has no

View Article Online
DOI: 10.1039/C8NJ05642K

obvious effect on the structure of gold NPs. In addition, catalysts Au-SnO_x/MCF and Au-MoO_x/MCF have no obvious diffraction peaks of transition metal species, probably due to the low loading of transition metal species and/or their uniform dispersion.

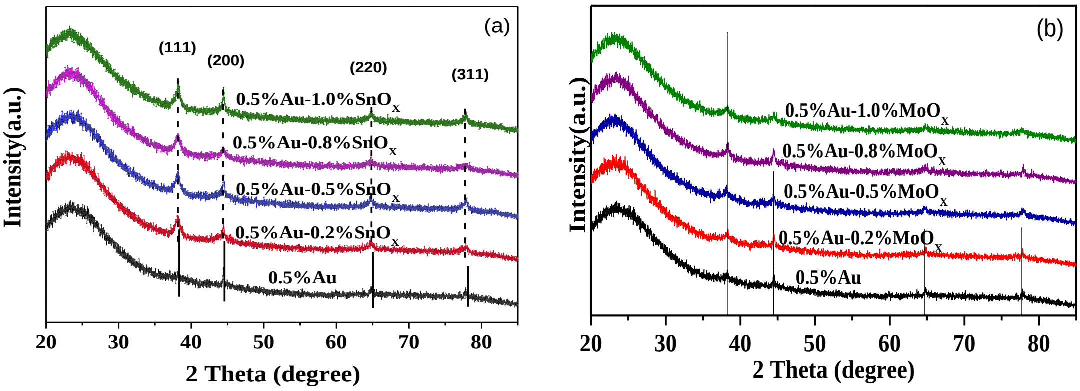

Fig. 3 XRD spectra of catalysts with different ratios, (a) Au-SnO_x/MCF and (b) Au-MoO_x/MCF catalysts.

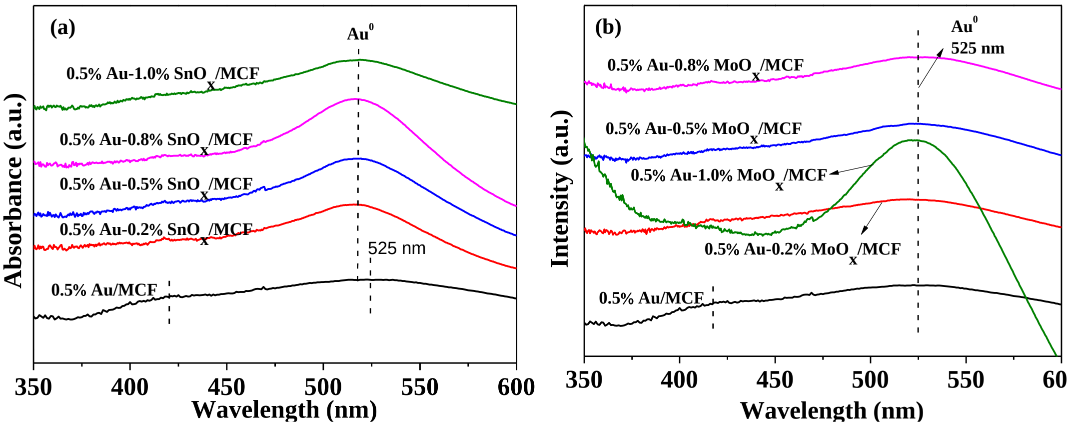

Fig. 4 UV-vis spectra of (a) Au-SnO_x/MCF and (b) Au-MoO_x/MCF catalysts.

Fig. 4 shows the UV-vis spectra of the catalysts. The 0.5%Au/MCF sample exhibits two broad peaks at ~420 nm and ~520 nm, respectively. According to literature,[31, 32] the peak at 420 nm corresponds to the partially charged Au_n clusters, while the peak at 520 nm is attributed to the surface plasmon resonance (SPR) of Au^0 NPs. When transition metal oxide is added, the peak at 520 nm is enhanced on catalysts Au-SnO_x/MCF with the increase of SnO_x content, while on catalysts Au-MoO_x/MCF, nearly no enhancement was detected until 1% of MoO_x added. This enhancement is attributed to the enhanced SPR of Au^0 NPs with gold NPs growing up, suggesting the strengthened interaction between transition metal oxide and Au NPs. In addition, compared to 0.5%Au/MCF, the peak at 520 nm shows a blue shift for Au-SnO_x/MCF, whereas its position is nearly unchanged for Au-MoO_x/MCF, indicating tin oxide has stronger interaction with Au NPs than molybdenum oxide. These results are consistent with the XRD and TEM data. On the other hand, as the transition metal oxides (SnO_x and MoO_x) content increases in the catalyst, the absorption peak at 420 nm weakens or reduces, due to the aggregation and growth of Au_n clusters as well as active surface coverage by SnO_x/MoO_x.

The surface chemical properties of Au/MCF, Au-SnO_x/MCF, and Au-MoO_x/MCF catalysts were revealed by XPS analysis and shown in Fig. 5 and ESI Fig. S1. As shown in Fig. 5(a), the typical Au^0 species with binding energies (BE) of 83.9 eV ($Au4f_{7/2}$) and 87.6 eV ($Au4f_{5/2}$) were observed on catalyst 0.5%Au/MCF.[32-34] When the transition metal oxides are introduced, a positive shift of Au 4f peaks for catalysts Au-SnO_x/MCF was observed, indicating the interaction of Au with Sn species. In the Sn 3d region as shown in Fig. 5b, signals positioned at 487.4 and 495.7eV were observed on 0.5%SnO_x/MCF which were ascribed to $3d_{5/2}$ and $3d_{3/2}$ photoelectrons of tetrahedrally coordinated SnO_2 species,[26] while on catalyst 0.5%Au-0.5%SnO_x/MCF the binding energy of $3d_{5/2}$ and $3d_{3/2}$ electrons shifted to higher value of 487.8 and 496.4 eV respectively, confirming the interaction between Au and Sn, leading to the formation of SnO_x species. As shown in Fig. S1, a slight positive shift of Au 4f binding energy on catalyst 0.5%Au-0.5%MoO_x/MCF was observed, indicating the weak interaction between Au and Mo species. However, the Mo 3d signal was undetectable even with a MoO_x loading of 2% on pure MoO_x/MCF sample, which is probably due to the low response of Mo species.

View Article Online
DOI: 10.1039/C8NJ05642K

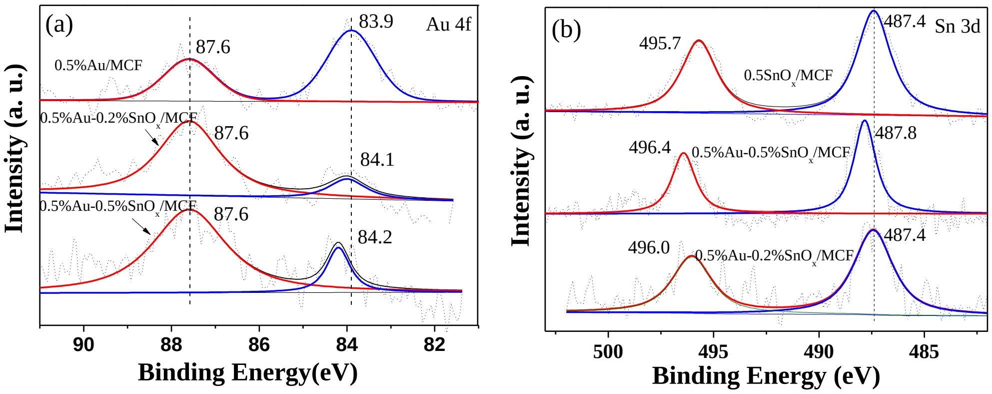

Fig. 5 Au(4f) and Sn (3d) XPS spectra of 0.5%Au/MCF, 0.5%Au-0.2%SnO$_x$/MCF, 0.5%Au-0.5%SnO$_x$/MCF and 0.5%SnO$_x$/MCF.

The elemental distribution of Au and Sn species has a profound effect on their catalytic performance and can be probed by STEM.[33, 34] Fig. 6 shows the representative STEM-HAADF images and the corresponding colour-coded EDS spectral maps of catalysts 0.5%Au-0.2%SnO$_x$/MCF and 0.5%Au-1.0%SnO$_x$/MCF. The aggregation of Au NPs was observed on both catalysts. EDS mapping shows that Sn (purple) elements are well distributed on the catalyst surface, and the energy dispersive line scan across NPs indicated the dispersion of Sn species aligned with Au, indicating the interaction between them.

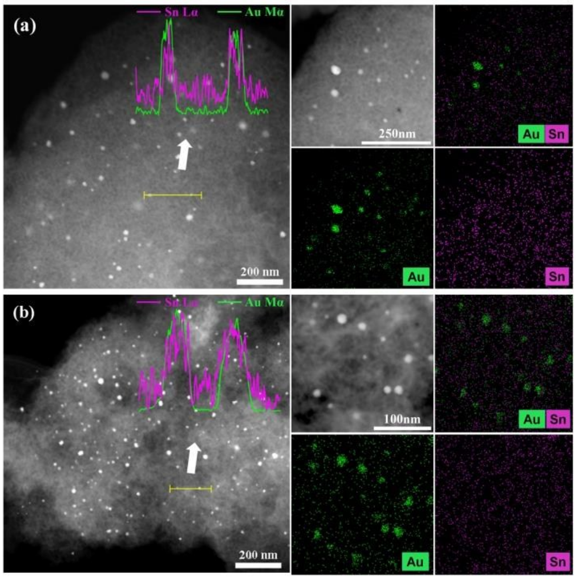

Fig. 6 Representative STEM-HADDF images of (a) 0.5%Au-0.2%SnOx/MCF and (b) 0.5%Au-1.0%SnOx/MCF (inset is the energy dispersive line scan across NPs using the Au-M and Sn L X-rays) and corresponding color-coded EDS spectral maps of Au (green), Sn (purple).

The results of energy dispersive line scan (inset of Fig.6) also reveals that the Sn species mainly dispersed on the surface of Au NPs, especially on catalyst 0.5%Au-1.0%SnO$_x$/MCF with higher SnO$_x$ loading, which shows a core-shell structure.[19]

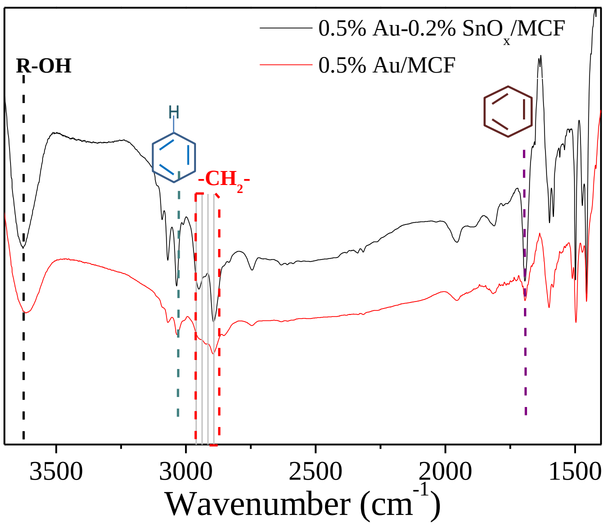

Fig.7 FTIR spectra of benzyl alcohol adsorbed on catalysts 0.5%Au-0.2%SnO$_x$/MCF and 0.5%Au /MCF.

In order to understand the states of benzyl alcohol-adsorbed catalyst, the infrared spectra of benzyl alcohol adsorbed 0.5%Au/MCF and 0.5%Au-0.2%SnO$_x$/MCF were measured and the results are shown in Fig. 7. The infrared spectrum of the benzyl alcohol molecules can be clearly confirmed from Fig. 7. [35] The FTIR characterization indicated that benzyl alcohol can be chemisorbed on gold catalyst. From Fig. 7, it was also observed that the peak intensity on catalyst 0.5%Au-0.2%SnO$_x$/MCF are much higher than those on catalyst 0.5%Au/MCF, indicating the benzyl alcohol adsorption capacity on catalyst 0.5%Au-0.2%SnO$_x$/MCF is higher than that on catalyst 0.5%Au /MCF.

In summary，high specific surface area and pore volume was maintained after introducing transition metal oxides to Au/MCF catalyst. XPS data revealed that electron transfer occurred between transition metals oxide and Au, furthermore, gold lattice distortion was detected on SnO_x promoted catalyst (Au-SnO_x/MCF) from XRD results, indicating the presence of strong interaction between SnO_x and Au NPs, which also led to the aggregation of gold NPs to some extent. EDS mapping results revealed the consistent dispersion of Au and Sn and the Sn species mainly distributed on the surface of Au NPs.

Catalytic performance

The catalytic performance of the Au/MCF, Au-SnO_x/MCF, and Au-MoO_x/MCF catalysts was evaluated in selective oxidation of benzyl alcohol with molecular oxygen. The conversion, selectivity and product distribution are summarized in Table 2. The pure Au catalyst (0.5%Au/MCF) exhibits a benzyl alcohol conversion of 15.4% with the primary products of 50% benzaldehyde, 31.5% benzoic acid, 6.8% toluene, and 8% benzyl benzoate. After introducing SnO_x to the Au/MCF catalyst, the benzyl alcohol conversion dramatically increased to 25.7% on catalyst 0.5%Au-0.2%SnO_x/MCF. The corresponding selectivity to benzaldehyde increases to 75.9%, while the benzoic acid selectivity decreases to 15.8%. However, further increase in tin content leads to the decrease of benzyl alcohol conversion to 9.1% on 0.5%Au-1%SnO_x/MCF, and the selectivity of benzaldehyde decreases to 51.1%, whereas the benzoic acid selectivity increases to 40.3%. This indicates that a low amount of tin oxide introduced results in a high catalytic activity, which is probably attributed to the strong interaction between SnO_x and gold NPs leading to the lattice distortion of Au NPs, but a higher amount of SnO_x may cover the Au active sites and leads to low catalytic activity. Meanwhile, with the increase of tin oxide content, the deep oxidation reaction is enhanced, resulting a higher benzoic acid selectivity on 0.5% Au-1.0%SnO_x/MCF (40.3%) than that on 0.5%Au-0.2%SnO_x/MCF (15.8%). This is because the presence of large amount of SnO_x on catalyst surface may act as an oxygen transfer bridge to enhance the deep oxidation of adsorbed benzaldehyde. It is worth noting that the addition of transition metal oxide as promoter switched off the toluene formation. Hutchings and co-workers applied[36] Pt as promoter to Au-Pd bimetallic catalyst to terminate the toluene formation from disproportionation reactions. They attributed this to the electronic or strain modification of Pt to the Au-Pd NPs. In this work, the electronic effect between Au and transition metal oxide (especially SnO_x) was certified by XPS analysis and the strain effect was confirmed by XRD analysis which would be further verified by DFT calculation.

Table 2 Catalytic performance of the catalysts in the oxidation of benzyl alcohol.

Samples	Conversion（%）	Selectivity（%）				
		Toluene	Benzaldehyde	Benzoic acid	Benzyl benzoate	others
Blank	2.1	15.4	45.6	27.1	6.8	5.1
0.5%Au/MCF	15.4	6.8	50	31.5	8	3.7
0.5%Au-0.2%SnO_x/MCF	25.7	0	75.9	15.8	6.3	2
0.5%Au-0.5%SnO_x/MCF	20.5	0	60.9	30.7	7.1	1.3
0.5%Au-0.8%SnO_x/MCF	13.6	0	54.7	37.4	7.3	0.6
0.5%Au-1%SnO_x/MCF	9.1	0	51.1	40.3	8.1	0.5
0.5%Au-0.2%MoO_x/MCF	13.0	0	78.3	6.0	6.7	9.0
0.5%Au-0.5%MoO_x/MCF	9.9	0	57.6	33.4	2.7	6.3
0.5%Au-0.8%MoO_x/MCF	5.6	0	55.0	45	0	0.0
0.5%Au-1%MoO_x/MCF	2.6	0	42.4	57.6	0	0

Reaction conditions: 50 mg of catalysts mixed with 10.8g of benzyl alcohol react at 110°C for 1h under an O_2 pressure of 8 bar.

As the content of molybdenum oxide in the catalyst increases, the conversion of benzyl alcohol decreases gradually. The conversion of benzyl alcohol on catalyst 0.5%Au-1.0%MoO_x/MCF is only 2.58%, due to large amount of active sites covered by molybdenum oxide, preventing the adsorption and activation of benzyl alcohol and O_2 on gold NPs, thus leading to low catalytic activity. Another possible reason may be that compared to tin oxide, the weaker interaction between molybdenum oxide and gold NPs (confirmed by the XRD and XPS results) hardly changes the structure of the gold surface, and thus no obvious improvement of catalytic activity was observed on catalyst Au-MoO_x/MCF. Similar benzaldehyde selectivity trend as catalyst Au-SnOx/MCF was observed on catalyst Au-MoO_x/MCF; that is, the benzaldehyde selectivity decreased with the increase of molybdenum oxide content, which is also explained as the enhanced deep oxidation reactions on transition metal oxides.

DFT calculation

To further explore the effect of transition metal oxides on gold catalysts for benzyl alcohol oxidation, DFT calculations were carried out. XPS results (as shown in Figure 5) and previously reported literature results[37, 38] suggested that when the transition metal contents are low, MoO_x and SnO_x tend to form high-valence oxides,

View Article Online
DOI: 10.1039/C8NJ05642K

SnO_2 and MoO_3, due to the sufficient oxidation in the air. Therefore, considering the representativeness and operability of modeling, SnO_2 and MoO_3 are selected as the models of our theoretical study. As shown in Fig. 8 and Fig. S2, when SnO_2 is adsorbed on Au(111), SnO_2 has a stronger interaction with Au(111) (E_{ads} = -2.48 eV) and induces obvious deformation of surface structure for Au(111), improving the activity of the Au(111) surface. This is because the deformation of Au NPs would lead to the presence of more low-coordinated Au sites as active sites for benzyl alcohol oxidation. However, for MoO_3/Au(111), the adsorption energy of MoO_3 on Au(111) is relative smaller (E_{ads} = -1.90 eV) and the surface structure of Au(111) has almost no change (Fig. 8 and Fig. S2), suggesting the weaker influence of MoO_3 on the structure of Au(111). In addition, more electron transfer between the Au(111) surface and SnO_2 (0.52 e) than MoO_3(0.30 e) further confirms the stronger interaction of SnO_2 and Au(111).

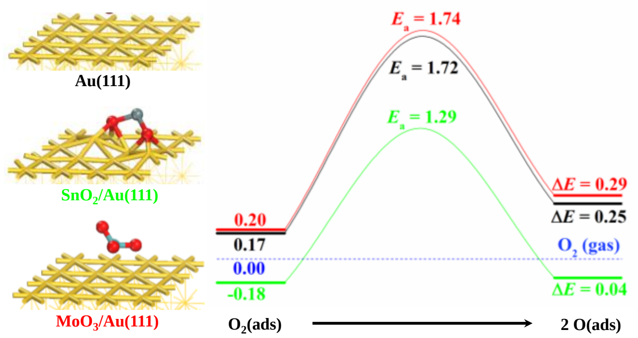

Fig. 8 Energy profiles for O_2 dissociation on the Au(111), SnO_2/Au(111), and MoO_3/Au(111) surfaces, with reaction energies ΔE, energy barriers E_a, and the gas phase O_2 chemical potential shown for reference (in eV).

Previous studies suggested that the rate-determining step in benzyl alcohol oxidation by molecular oxygen is the activation of O_2 [25, 27-29] on Au NP catalyst. Therefore, the adsorption and dissociation of O_2 were calculated on the Au(111), SnO_2/Au(111), and MoO_3/Au(111) surfaces in this work. On the pure Au(111) surface, an oxygen molecule preferably adsorbs on the Au_2-bridge site with the O-O bond length of 0.1274 nm, while an oxygen atom prefers to adsorb at Au_3-fcc site (see Fig. S3). However, Au(111) is inert for oxygen adsorption as mirrored by the positive adsorption energies of 0.17 eV for molecular O_2 and 0.04 eV for atomic O (relative to 1/2 O_2 in gas phase). This situation is in accordance with previous experimental and theoretical studies.[39] After introduction of SnO_2 on Au(111), both the molecular O_2 and atomic O prefer to adsorb at the SnO_2–Au interface (see Fig. S3). The adsorption energy of molecular O_2 is strengthened to -0.18 eV, and the O-O bond length is stretched to 0.1356 nm. In addition, the adsorption energy of atomic O is also strengthened to -0.46 eV, relative to 1/2 O_2 in gas phase. The enhanced adsorption of oxygen suggests SnO_2/Au(111) has a higher catalytic activity toward O_2 activation compared to Au(111). On MoO_3/Au(111), the adsorption energies of molecular O_2 and atomic O are calculated to be 0.21 and 0.08 eV, respectively, and the O-O bond length for adsorbed O_2 is 0.1261 nm, suggesting the lower activity of MoO_3/Au(111) toward O_2 than pure Au(111). This may be caused by the more electrostatic repulsion of MoO_3 group with oxygen on MoO_3/Au(111).

Table 3 Adsorption energies, E_{ads} (in eV) of O_2 and O as well as O-O bond length $d_{O\text{-}O}$ (in nm) of adsorbed O_2 on catalyst surfaces.

Catalysts	$d_{O\text{-}O}$	$E_{ads}(O_2)$	$E_{ads}(O)^a$
Au(111)	0.1274	0.17	0.04
SnO_2/Au(111)	0.1356	-0.18	-0.46
MoO_3/Au(111)	0.1261	0.21	0.08

[a] Energies are relative to the total energy of 1/2 gaseous O_2 molecule and the clean catalyst.

The energy profiles for the O_2 dissociation into 2O on the Au(111), SnO_2/Au(111), and MoO_3/Au(111) surfaces are shown in Fig. 8. The optimized geometries for the initial states, transition states, and final states involved in the reaction are presented in Fig. S4. As shown in Fig. 8, the dissociation of O_2 into 2O on pure Au(111) is endothermic by 0.25 eV, and the reaction is impeded by a high energy barrier of 1.72 eV. When SnO_2 is introduced to the Au(111) surface, the O_2 dissociation barrier is reduced to 1.29 eV and the reaction is only slightly endothermic by 0.04 eV, further confirming that tin oxide can enhance the reactivity of O_2 on the Au surface and thus improve the catalytic performance for benzyl alcohol oxidation. However, compared to pure Au(111), MoO_3/Au(111) has a higher O_2 dissociation barrier of 1.74 eV and stronger endothermicity of 0.29 eV. Therefore, introduction of molybdenum oxide reduces the catalytic activity of gold towards O_2 and thus shows a lower catalytic activity in benzyl alcohol oxidation.

Conclusions

In this study, Au-SnO_x/MCF and Au-MoO_x/MCF catalysts were synthesized with transition metal oxides (SnO_x and MoO_x) as promoters. When a small amount of SnO_x was introduced, a strong interaction between SnO_x and Au NPs was observed, which leads to the deformation of the surface structure of Au NPs, confirmed by the characterization results as well as DFT calculations. The distortion of Au NPs results in the formation of more low-coordinated Au active sites and thus the catalytic performance for benzyl alcohol oxidation is improved. While introducing a high content of SnO_x into Au-SnO_x/MCF catalyst, the surface of the Au NPs are covered by SnO_x species, which prevents the adsorption of reactants, resulting in a decrease of catalytic performance. On the other hand, because of the weaker interaction between MoO_x and Au NPs and partial coverage of active sites, Au-MoO_x/MCF catalysts exhibited a low catalytic activity for benzyl alcohol oxidation. The characterization results revealed the presence of electronic and strain modification of transition metal oxide to Au NPs, while DFT calculation visualized these results. Therefore, this work provides an effective route for promoters screening through combing the experimental results with DFT calculation, which will shed light on the design of transition metal/transition metal oxide promoted noble metal catalysts with improved catalytic performance.

Experimental

Materials

$HAuCl_4 \cdot 3H_2O$ (Aladdin), stannous chloride ($SnCl_2 \cdot 2H_2O$, Sinopharm Chemical), ammonium molybdate ($(NH_4)_6Mo_7O_{24} \cdot 4H_2O$, Sinopharm Chemical), 1,3,5- trimethylbenzene (C_9H_{12}, Sinopharm Chemical), triblock co-polymer $PEO_{20}PPO_{70}PEO_{20}$ (P123, Sigma-Aldrich), mercaptopropyltrimethoxysilane (MPTMS, 97%, Aladdin), tetraethoxysilane ($C_8H_{20}O_4Si$, 98%, Sinopharm Chemical), benzyl alcohol (99.99%, Sinopharm Chemical), absolute ethanol (99.98%, Sinopharm Chemical), and hydrochloric acid (37%, Sinopharm Chemical) were used as received without further purification.

Catalysts synthesis

Synthesis of Au/MCF

The synthesis procedure of Au/MCF catalysts was similar to that reported in our previous work.[12] In a typical synthesis, P123 (4 g) was first dissolved into a mixture of 37% HCl (5 mL) and deionized water (65 mL) at room temperature. Then, 1,3,5-trimethylbenzene (3g) was introduced to the clear solution as a pore-foaming agent and stirred at 38 ^oC for 2 h, followed by dropwise adding of MPTMS (0.57 g) and tetraethoxysilane (9.2 g) to the mixture. After that, $HAuCl_4 \cdot 3H_2O$ (3.55 mL, 0.02 mol/L) was added into the synthesis system under stirring, and the mixture was further crystallized at 100 ^oC for 24 h in an autoclave. Finally, the as-synthesized sample was washed with deionized water and ethanol, sequentially, dried in a vacuum oven at 80 ^oC for 12 h, and then calcined in air at 550 ^oC for 6 h. The resulting sample was designated as 0.5%Au/MCF, where 0.5% is the weight percentage of Au.

Synthesis of Au–SnO_x/MCF and Au–MoO_x/MCF

The 0.5%Au/MCF sample (2 g) was added to a certain amount of stannous chloride solution (0.1 mol/L) and stirred to a gelatinous mixture. The gelatinous mixture was dried in a vacuum oven at 100 ^oC for 12 h, and then calcined in air at 300 ^oC for 4 h to obtain nAu–$m$$SnO_x$/MCF, where n and m represent the weight percentage of Au and SnO_x, respectively. The nAu–$m$$MoO_x$/MCF catalysts were prepared by the same method as that for nAu-$m$$SnO_x$/MCF except that stannous chloride solution (0.1 mol/L) was replaced by ammonium molybdate solution (0.1 mol/L).

Characterization

The crystalline structure of the samples was characterized by measuring X-ray diffraction (XRD) patterns on an X'Pert PRO MPD instrument with a Cu $K\alpha$ radiation (λ = 0.15418 nm) at 35 kV and 40 mA. Transmission Electron Microscope (TEM) was performed to examine the morphologies of the samples using JEOL JEM 2010 microscope operated at 200 kV. The particle size distribution obtained by counting 150-200 particles and the average particle size of samples were analyzed from TEM data. Metal loadings in the catalysts were determined by inductively coupled plasma optical emission spectroscopy (ICP-OES) using a VISTA-MPX Varian system.

The textural properties of the samples were analyzed from nitrogen adsorption–desorption isotherms measured at 77 K by a surface area and porosity analyzer (Micromeritics, TriStar 3000). The Brunauer-Emmett-Teller (BET) equation was used to calculate the specific surface area in the relative pressure P/P_0 of 0.05-0.25, while the Barrett-Joyner-Halenda (BJH) equation was used to calculate the pore size distribution from the desorption branch of isotherms. In addition, the pore volume of catalysts was obtained at P/P_0 of 0.989. The surface properties of the samples were analyzed using X-ray photoelectron spectroscopy (XPS) and the solid ultraviolet-visible (UV-vis) absorption spectrophotometer. XPS data were obtained on a Thermo-VG Scientific K-Alpha spectrometer equipped with an Al anode (Al $K\alpha$ = 1486.6 eV) and the binding energies were determined utilizing the C1s spectrum as reference at 284.5 eV. The UV-vis absorption spectra were acquired on a HitachiU-4100 UV-vis-NIR scanning spectrophotometer by using $BaSO_4$ as an internal reference. Scanning transmission electron microscopy (STEM) high angle annular dark field (HAADF) images and X-ray energy dispersive spectra (XEDS) of the metallic particles were obtained using a JEOL JEM-2100F with an accelerating voltage of 200kV. The Fourier infrared diffuse reflection spectra of benzyl alcohol adsorption were recorded on a NEXUS FTIR (Thermo Fisher Scientific, USA) using degassed pure catalyst as blank. Prior to the measurement, the samples were degassed in a vacuum at 573 K for 2 h to ensure the removal of moisture. The degassed samples were soaked in benzyl alcohol for 24h and dried in vacuum oven for 8 h. And then the samples were degassed in a vacuum at 573 K for 3 h to remove the physically adsorbed benzyl alcohol. The FT-IR spectra were finally recorded from 4000 to 400 cm^{-1} using the average record of 64 times scanning.

View Article Online
DOI: 10.1039/C8NJ05642K

Calculation models and method

All density functional theory (DFT) calculations were carried out using the Perdew–Burke–Ernzerhof (PBE) functional with the generalized gradient approximation (GGA) method [40] implemented in the $DMol^3$ code [41, 42] of Material Studio. The metal ion cores were treated with density functional semicore pseudopotential (DSPP), while the valence electrons were calculated using the double numerical plus polarization (DNP) basis set. All calculations were performed using spin-polarization with the convergence criteria of 1×10^{-5} Ha for energy change, 2×10^{-3} Ha Å^{-1} for max force, and 5×10^{-3} Å for displacement.

The Au(111) surface was built using a periodic four-layer slab with a p(4 × 4) unit cell. Periodic images of the slab were separated by a 15 Å vacuum gap, and a 5×5×1 k points was sampled in the reciprocal space. In the calculation process, the atoms in the two upmost layers as well as adsorbates were fully relaxed, while those in the two bottom layers were fixed to the bulk positions. The SnO_2/Au(111) and MoO_3/Au(111) models were built via SnO_2 and MoO_3 adsorbed at the lowest energy position of the Au(111) surface, respectively. The adsorption energy (E_{ads}) was calculated by $E_{ads} = E_{adsorbate/substrate} - (E_{adsorbate} + E_{substrate})$, where $E_{adsorbate/substrate}$ is the total energy of the substrate with an adsorbed molecule, and $E_{adsorbate}$ and $E_{substrate}$ are the energies of the free adsorbate and the clean substrate, respectively.

Catalytic Tests

The selective oxidation of benzyl alcohol with O_2 as oxidant was performed in a 100 mL autoclave with polytetrafluoroethylene lining (Model: SLM100, Beijing Easychem Science and Technology Development Company, China). In the catalytic test, benzyl alcohol

(10.8 g) and solid catalyst (50 mg) were added into the reactor. Then, the autoclave was sealed, purged with O_2 for three times, and then heated to 110 °C. The reaction was carried out for 1 h under the O_2 pressure of 0.8 Mpa. After reaction, the reactor was cooled in an ice bath to 30 °C and the pressure was released. The reaction products were separated by centrifuge and analyzed using a gas chromatogram (Agilent 6870) equipped with an FID detector and a DB-1 column (30*0.32*0.25).

Conflicts of interest

There are no conflicts to declare.

Acknowledgements

This work was supported by National Natural Science Foundation of China (51601223, 21805307), the Fundamental Research Funds for the Central Universities (17CX05018, 17CX02056), PetroChina Innovation Foundation (2018D-5007-0504), State Key Laboratory of Heavy Oil Processing（SKLZZ-2017008) and Qingdao Postdoctoral Applied Research Project (BY20170215).

References

1. N. Gogoi, P. Bordoloi, G. Borah and P. K. Gogoi, *Cataly. Lett.*, 2017, **147**, 539.
2. C. Lavenn, A. Demessence and A. Tuel, *J. Catal.*, 2015, **322**, 130.
3. J. Luo, H. Yu, H. Wang, H. Wang and F. Peng, *Chem. Eng. J.*, 2014, **240**, 434.
4. G. Zhao, X.-P. Wu, R. Chai, Q. Zhang, X.-Q. Gong, J. Huang and Y. Lu, *Chem. Commun.*, 2015, **51**, 5975.
5. G. Zhao, F. Yang, Z. Chen, Q. Liu, Y. Ji, Y. Zhang, Z. Niu, J. Mao, X. Bao and P. Hu, *Nat. Commun.*, 2017, **8**, 14039.
6. M. Misono, *Chem. Commun.*, 2001, **13**, 1141.
7. P. M. Rao, A. Wolfson, S. Kababya, S. Vega and M. V. Landau, *J. Catal.*, 2005, **232**, 210.
8. N. Mizuno and M. Misono, *Chem. Rev.*, 1998, **98**, 199.
9. M. Haruta, T. Kobayashi, H. Sano and N. Yamada, *Chem. Lett.*, 1987, **16**, 405.
10. I. Nakamura, A. Takahashi and T. Fujitani, *Catal. Lett.*, 2009, **129**, 400.
11. X. Deng, B. K. Min, A. Guloy and C. M. Friend, *J. Am. Chem. Soc.*, 2005, **127**, 9267.
12. P. Wu, P. Bai, K. P. Loh and X. Zhao, *Catal. Today*, 2010, **158**, 220.
13. N. Dimitratos, J. A. Lopez-Sanchez, D. Morgan, A. Carley, L. Prati and G. J. Hutchings, *Catal. Today*, 2007, **122**, 317.
14. N. Dimitratos, J. A. Lopez-Sanchez, D. Morgan, A. F. Carley, R. Tiruvalam, C. J. Kiely, D. Bethell and G. J. Hutchings, *Phys. Chem. Chem. Phys.*, 2009, **11**, 5142.
15. F. Galvanin, M. Sankar, S. Cattaneo, D. Bethell, V. Dua, G. J. Hutchings and A. Gavriilidis, *Chem. Eng. J.*, 2018, **342**, 196.
16. A. Savara, C. E. Chan-Thaw, J. E. Sutton, D. Wang, L. Prati and A. Villa, *ChemCatChem*, 2017, **9**, 253.
17. T. Yoskamtorn, S. Yamazoe, R. Takahata, J.-i. Nishigaki, A. Thivasasith, J. Limtrakul and T. Tsukuda, *ACS Catal.*, 2014, **4**, 3696.
18. J. H. Carter, S. Althahban, E. Nowicka, S. J. Freakley, D. J. Morgan, P. M. Shah, S. Golunski, C. J. Kiely and G. J. Hutchings, *ACS Catal.*, 2016, **6**, 6623.
19. T. A. G. Silva, E. Teixeira-Neto, N. Lopez and L. M. Rossi, *Sci. Rep.*, 2014, **4,** 5766.
20. H. Wang, C. Wang, H. Yan, H. Yi and J. Lu, *J. Catal.*, 2015, **324**, 59.
21. F. Gomez-Villarraga, J. Radnik, A. Martin and A. Koeckritz, *J. Nanopart. Res.*, 2016, **18,** 235.
22. C. M. Olmos, L. E. Chinchilla, E. G. Rodrigues, J. J. Delgado, A. B. Hungría, G. Blanco, M. F. Pereira, J. J. Órfão, J. J. Calvino and X. Chen, *Appl. Catal. B: Environ.*, 2016, **197**, 222.
23. P. J. Miedziak, Q. He, J. K. Edwards, S. H. Taylor, D. W. Knight, B. Tarbit, C. J. Kiely and G. J. Hutchings, *Catal. Today*, 2011, **163**, 47.
24. Y. Dong, H. Zhang, W. Li, M. Sun, C. Guo and J. Zhang, *J. Ind. Eng. Chem.*, 2016, **35**, 177.
25. Q. Jia, D. Zhao, B. Tang, N. Zhao, H. Li, Y. Sang, N. Bao, X. Zhang, X. Xu and H. Liu, *J. Mater. Chem. A*, 2014, **2**, 16292.
26. T. Lu, X. Fu, L. Zhou, Y. Su, X. Yang, L. Han, J. Wang and C. Song, *ACS Catal.*, 2017, **7**, 7274.
27. C. D. Pina, E. Falletta and M. Rossi, *J. Catal.*, 2008, **260**, 384.
28. W. Li, A. Wang, X. Liu and T. Zhang, *Appl. Catal. A: Gen.*, 2012, **433**, 146.
29. W. Yi, W. Yuan, Y. Meng, S. Zou, Y. Zhou, W. Hong, J. Che, M. Hao, B. Ye and L. Xiao, *ACS Appl. Mate. Inter.*, 2017, **9**, 31853.
30. P. Schmidt-Winkel, W. W. Lukens, D. Zhao, P. Yang, B. F. Chmelka and G. D. Stucky, *J. Am. Chem. Soc.*, 1999, **121**, 254.
31. J. Sá, S. F. R. Taylor, H. Daly, A. Goguet, R. Tiruvalam, Q. He, C. J. Kiely, G. J. Hutchings and C. Hardacre, *ACS Catal.*, 2012, **2**, 552.
32. P. Wu, Z. Xiong, K. P. Loh and X. Zhao, *Catal. Sci. Technol.*, 2011, **1**, 285.
33. R. Tiruvalam, J. Pritchard, N. Dimitratos, J. Lopez-Sanchez, J. Edwards, A. Carley, G. Hutchings and C. Kiely, *Faraday Discuss.*, 2011, **152**, 63.
34. C. M. Olmos, L. E. Chinchilla, A. Villa, J. J. Delgado, H. Pan, A. B. Hungria, G. Blanco, J. J. Calvino, L. Prati and X. Chen, *Appl. Catal. A-Gen.*, 2016, **525**, 145.
35. S. Higashimoto, N. Kitao, N. Yoshida, T. Sakura, M. Azuma, H. Ohue and Y. Sakata, *J. Catal.*, 2009, **266**, 279.
36. Q. He, P. J. Miedziak, L. Kesavan, N. Dimitratos, M. Sankar, J. A. Lopez-Sanchez, M. M. Forde, J. K. Edwards, D. W. Knight, S. H. Taylor, C. J. Kiely and G. J. Hutchings, *Faraday Discuss.*, 2013, **162**, 365.
37. L. L. M. Wang, H. Luo, S. Zhang, H. Zhang, K. Javaid, H. Cao, *IEEE Elect. Device L.*, 2016, **37**, 422.
38. H. J. K. E. J. Lim, W. B. Kim,, *Catal. Commun.*, 2012, **25**, 74.
39. M. M. Montemore, M. A. van Spronsen, R. J. Madix and C. M. Friend, *Chem. Rev.*, 2017, **118**, 2816.
40. J. P. Perdew, K. Burke and M. Ernzerhof, *Phys. Rev. Lett.*, 1996, **77**, 3865.
41. B. Delley, *J. chem. phys.*, 1990, **92**, 508.
42. B. Delley, *J. chem. phys.*,2000, **113**, 7756.

Table of Content